Surface Salt Bridges, Double-Mutant Cycles, and Protein Stability: an Experimental and Computational Analysis of the Interaction of the Asp 23 Side Chain with the N-Terminus of the N-Terminal Domain of the Ribosomal Protein L9†

Donna L. Luisi,[‡,§,||] Christopher D. Snow,[§,||,⊥] Jo-Jin Lin,[‡] Zachary S. Hendsch,[#] Bruce Tidor,*[,#] and Daniel P. Raleigh*[,‡,▽]

Department of Chemistry, State University of New York at Stony Brook, Stony Brook, New York 11794-3400, Biological Engineering Division and Department of Electrical Engineering and Computer Science, Massachusetts Institute of Technology, Room NE-725, Cambridge, Massachusetts 02139-4307, and Graduate Program in Biophysics and Graduate Program in Biochemistry and Structural Biology, State University of New York at Stony Brook, Stony Brook, New York 11794

Received November 19, 2002; Revised Manuscript Received April 18, 2003

ABSTRACT: Experimental and theoretical double-mutant cycles have been used to investigate a salt bridge in the N-terminal domain of the protein L9. Aspartic acid 23 is the only acidic residue involved in a well-defined pairwise interaction, namely, a partially solvent-exposed salt bridge with the protonated N-terminus of the protein. Mutations were studied in which Asp 23 was substituted by alanine, asparagine, and nitrile alanine. Interactions with the N-terminus were probed by comparisons between proteins with a protonated and acetylated N-terminus. The mutants were all folded, and the structures were unchanged from wild type as judged by CD and 2-D NMR. The coupling free energy between the N-terminus and the side chain of Asp 23 measured through double-mutant cycle analysis was favorable and ranged from -0.7 to -1.7 kcal mol^{-1}, depending upon the set of mutants used. This relatively large coupling free energy for a surface salt bridge likely arises from geometric factors that reduce the entropy loss associated with salt-bridge formation and from structural relaxation in the mutants. Coupling free energies computed with continuum electrostatic calculations agreed well with the experimental values when full account was taken of all potential interactions, particularly those involving Asp 23 and the acetylated N-terminus as well as interactions with solvent. The measured and calculated coupling free energy decreased only slightly when the salt concentration was increased from 100 to 750 mM NaCl. The calculations suggest that the coupling free energy between D23 and the N-terminus measured through the experimental double-mutant cycle analysis is significantly smaller than the actual interaction free energy between the groups in the wild-type structure because of the inapplicability of assumptions frequently used to interpret double-mutant cycles.

The role of electrostatic interactions in protein stability and folding is a topic of great interest (*1*−*9*). Particular attention has been focused on the role of salt bridges in protein stability (*10*−*18*). Recent experimental and computational studies have suggested that, in some cases, salt bridges may not always provide substantial stability enhancements beyond that conferred by hydrophobic interactions involving groups of similar size (*14*, *16*, *18*). A number of studies have investigated the role of increased or enhanced electrostatic interactions in thermophilic proteins as compared to their mesophilic counterparts as a possible source of increased thermostability (*19*−*23*). Electrostatic interactions involving surface residues have also received considerable attention as target sties for mutations designed to rationally stabilize proteins (*24*−*28*).

Electrostatic interactions can be studied by a variety of techniques. A particularly useful approach is to employ double-mutant cycles to measure the coupling free energy between the groups by mutating the residues of interest separately and concurrently (*10*, *29*). Under ideal circumstances, the coupling free energy can be associated with the free energy of interaction between the residues in the folded protein, but this requires that there be no significant structural rearrangement caused by the mutations, that other interactions are additive from the single mutants to the double mutants, and that no significant changes in unfolded state interactions occur. Complications arise in interpretation if any of these conditions are violated. To distinguish experiment from interpretation, here we will use the term coupling free energy to describe the result of double-mutant cycle analysis (whether experimental or theoretical) and the term interaction free energy to describe a direct interaction between a pair

† This work was supported by NSF Grant MCB-0079406 to D.P.R. and by NIH Grant GM55758 to B.T.

* Authors to whom correspondence should be addressed. (D.P.R.) Telephone: (631) 632-9547. Fax: (631) 632-7960. E-mail: Draleigh@notes.cc.sunysb.edu. (B.T.) Telephone: (617) 253-7258. Fax: (617) 252-1816. E-mail: tidor@ai.mit.edu.

‡ State University of New York at Stony Brook.

§ Current address: Wyeth Biopharma, 1 Burtt Rd., Andover, MA 01810.

|| These authors contributed equally to this work.

⊥ Current address: Department of Biophysics, Stanford University, Stanford, CA 94305.

Massachusetts Institute of Technology.

▽ State University of New York at Stony Brook.

10.1021/bi027202n CCC: $25.00
Published on Web 05/20/2003

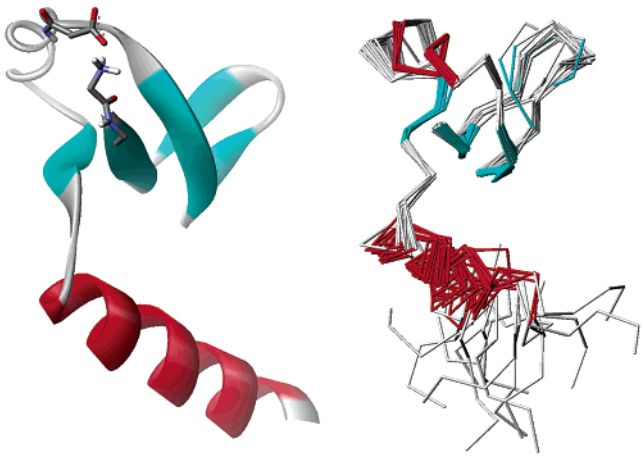

FIGURE 1: Structure of NTL9 with the side chain of Asp 23 and the free N-terminus shown in ball-and-stick format. (A) Combined NMR and X-ray structure. (B) 18 member NMR ensemble. Drawn with Weblab Viewer Lite (MSI Inc).

of functional groups within a protein. Only if circumstances are ideal can a coupling free energy measured through double-mutant cycle analysis be associated with an interaction free energy. The interaction free energy measured in this way is sometimes equated with the net contribution that the salt bridge makes to the stability, but this is misleading since the double-mutant cycle analysis attempts to cancel the desolvation penalty of each of the side chains (*14*). Said another way, the ideal double-mutant cycle result is the screened interaction free energy of the bridging side chains in the folded state, which is clearly only part of the effect of these residues on protein folding. Typically, only modest free energy values are measured for salt bridges involving surface residues, as assessed through double-mutant cycles and pK_a shifts (*5*, *6*, *10*−*13*, *17*, *29*). Notable exceptions are the partially buried salt bridge in T4 lysozyme, which has a measured coupling free energy of −3 to −5 kcal mol^{-1}and a surface salt bridge in a hyperthermophilic rubredoxin variant, which has a measured coupling free energy of −1.5 kcal mol^{-1} (*30*−*32*).

The usefulness of double-mutant cycles is that, in principle, they allow the isolation of specific interactions in the absence of background or context effects. Here, we use double-mutant cycle analysis to investigate the role of a partially exposed salt bridge in the stability of the N-terminal domain of the ribosomal protein L9 (NTL9).[1] Through a detailed comparison of experiment and calculation, assumptions generally used to interpret double-mutant cycles were tested. NTL9 is a small mixed $\alpha-\beta$ protein that folds in a two-state fashion (Figure 1) (*33*, *34*). It is a basic protein containing 12 basic residues and six acidic residues. The acidic residues are well-distributed throughout the 3-D structure and titrate independently of each other (*35*). A well-defined salt bridge is formed between Asp 23 and the free N-terminus. In the joint X-ray/NMR structure, the terminal nitrogen is 2.66 Å from the proximal carboxylate oxygen of the Asp 23 side chain. These groups lie at the surface of the protein, but they are not completely solvent accessible. The protonated N-terminus has a solvent accessibility of only 2.5%, while the Asp side chain is 75% accessible. The two groups are well-isolated from other charged residues. Only one basic group, Lys-12 at 8 Å distance, is within 14 Å of the N-terminus, and D23 is the only acidic group within 10 Å of the N-terminus. E38 is the only acidic residue within 14 Å of D23. The ϵ-amino group of K2 is 9 Å from the D23 side chain, while all other basic residues are more than 11 Å distant.

MATERIALS AND METHODS

Materials. PAL resin was purchased from Perseptive Biosytems (Framingham, MA). HATU was purchased from Advanced Chemtech (Louisville, KY). Fmoc-protected amino acids were purchased from Advanced Chemtech and Perseptive Biosystems. D_2O and sodium 3-trimethylsilyl (2,2,3,3-d_4) propionate were purchased from Cambridge Isotope Laboratories (Andover, MA). All other solvents and reagents were purchased from Fisher Scientific (Springfield, NJ).

Peptide Synthesis and Purification. The proteins were prepared by solid-phase synthesis using a Millipore 9050 Plus automated peptide synthesizer and standard Fmoc chemistry. The proteins were purified by reverse phase high-pressure liquid chromatography (HPLC) using a C4 preparative column. All of the proteins were greater than 95% pure as judged by analytical HPLC. Variants containing nitrile alanine (in which a cyano group replaces the side chain carboxylate) or asparagine at position 23 were generated by solid-phase peptide synthesis. Incorporating Fmoc-Asn without side chain protection at position 23 generated the nitrile Ala analogue via the dehydration of the side chain during Fmoc removal. A mixture of peptides resulted. One contained nitrile alanine at position 23, and the other contained an asparagine. The two were separated by reverse phase HPLC.

The identities of the proteins were confirmed by matrix assisted laser desorption ionization time-of-flight mass spectroscopy (MALDI-TOF). The calculated and observed molecular weights were NTL9 calculated 6218 Da, observed 6217 Da; the acetylated variant (NTL9$_{Ac}$) calculated 6260 Da, observed 6263 Da; NTL9 D23N calculated 6217 Da, observed 6217 Da; the variant with an Asn at residue 23 and an acetylated N-terminus (NTL9 D23N$_{Ac}$) calculated 6259 Da, observed 6261 Da; NTL9 D23A calculated 6191 Da, observed 6183 Da; D23A$_{Ac}$ calculated 6233 Da, observed 6225 Da; the variant with the side chain carboxylate of Asp 23 replaced by nitrile (NTL9 D23CN) calculated 6199 Da, observed 6195 Da; and NTL9 D23CN$_{Ac}$ calculated 6241 Da, observed 6244 Da.

Circular Dichroism Spectroscopy. Circular dichroism (CD) experiments were performed on an Aviv Model 62A DS CD spectrometer equipped with a Peltier temperature control system. All of the CD experiments were performed using a buffer of 100 or 750 mM sodium chloride and 10 mM sodium phosphate (pH 5.4); protein concentrations were in the range of 25−425 μM. Temperature denaturation experi-

[1] Abbreviations: 2-D, two-dimensional; CD, circular dichroism; Fmoc, *N*α-9-fluorenylmethyloxycarbonyl; HATU, *O*-(7-azabenzotriazole-1-yl)-1,1,3,3-tetramethyluronium hexafluorophosphate; HPLC, high-pressure liquid chromatography; MALDI-TOF, matrix assisted laser desorption ionization time-of-flight; NMR, nuclear magnetic resonance; NTL9, N-terminal domain of the ribosomal protein L9 from *Bacillus stearothermophilus* comprising residues 1−56; NTL9Ac, N-terminal domain of the ribosomal protein L9 with an acetylated N-terminus; NTL9$_{D23CN}$, N-terminal domain of the ribosomal protein L9 with Asp-23 replaced by an nitrile alanine; PAL, polystyrene Fmoc support for peptide amides; TFA, trifluoroacetic acid; TOCSY, total correlation spectroscopy.

ments were performed over the range of 2−98 °C, with two degree steps and a 45 s equilibration time and were followed at 280 nm. Thermal denaturation was greater than 90% reversible. Urea denaturation experiments were followed at a wavelength of 222 nm. The concentration of urea was determined by refractometry (*36*). The thermal and chemical unfolding curves were fit to the standard expressions for two-state transitions using a method that explicitly accounted for the baselines (*36*).

NMR Spectroscopy. NMR experiments were performed using a Varian INOVA 500 MHz spectrometer. The pK_a of the Asp 23 in NTL9 Ac was determined by recording a set of nine TOCSY spectra between pH 2.2 and 6.8 in H_2O. The chemical shifts of the Asp 23 β-protons could be followed throughout the titration. Plots of chemical shift versus pH were fit to the standard Henderson−Hasselbalch equation.

Modeling. Two sets of structures were used in the calculations. The first was a single structure of NTL9 determined though a combination of X-ray crystallography, and the second was the 18-member NMR ensemble. Models for the mutant proteins were derived by building the appropriate groups into the wild-type structures and minimizing the energy using the CHARMM program (Figure 1) (*37*). Changes to the wild-type structure to generate models of the mutant NTL9 were conservative. Namely, the model for D23A was created by simple truncation. Models for D23N and D23CN were created from D23A by building new atoms onto the β-carbon at position 23 and minimizing only the new residue. The model for $D23A_{Ac}$ was generated from the D23A model structure by building the acetyl group, rotating the acetyl group to optimize potential hydrogen bonding interactions of the amide hydrogen with the carbonyl of residue 21, and adjusting the torsions of Asn 20 to remove a steric clash with the increased N-terminal bulk while forming potential hydrogen bonds with the backbone, Lys 2, and the new acetyl. Finally, this structure was allowed to relax by minimizing the acetyl and Asn 20. Models for $NTL9_{Ac}$, $D23N_{Ac}$, and $D23CN_{Ac}$ were built starting from the $D23A_{Ac}$ model by building new atoms onto the β-carbon of position 23 in standard geometry and minimizing the new residue. The energy associated with the change in Asn 20 conformation was not calculated because it canceled in any double-mutant cycle that included a pair of acetylated models. Models of the mutant structures built from the single combined X-ray/NMR structure are shown in Figure 2.

Molecular mechanics parameters were taken from the CHARMM PARAM19 set where possible and augmented with quantum mechanical calculations for groups outside of PARAM19 (*37*). For the nitrile alanine side chain, parameters were derived through the use of constrained quantum mechanical geometry optimization and restrained electrostatic potential fitting. Namely, the geometry optimization constrained the backbone torsions to the values seen in the single protein model, while the torsions involving side chain atoms were optimized. The fixed backbone was used to ensure that the product was applicable to the protein site. The model for the nitrile alanine residue replaced the α-carbon of adjacent residues with freely rotating methyl groups. The geometry optimization was performed using Hartree−Fock with the 6-31G** basis set using the Jaguar program (Schrodinger, Inc., Portland, OR, Jaguar 3.5, 1998). A Gaussian 98 implementation of 6-31 + G* was used to calculate the electrostatic surface potential on a grid (Gaussian 98, Revision A.7, Gaussian, Inc., Pittsburgh PA, 1998). A two-stage restrained electrostatic potential fitting procedure was used to assign atomic charges as described by Bayly et al. (*38*). The resulting charge distribution was adjusted slightly to balance charge for the residue while emulating the standard backbone charges from both the PARSE and the CHARMM parameter set (Table 1). Bond lengths and angles were taken from the geometry optimization. Other parameters were estimated from values in PARAM19. The parametrization is shown in Table 1.

Electrostatic Calculations. A modified version of the DELPHI computer program was used for continuum electrostatic calculations as described previously (*39*−*41*). The PARSE parameter set of charges and atomic radii augmented with charges derived quantum mechanically for nitrile alanine were used (*42*). The protein dielectric constant was 4, the solvent dielectric constant was 80, and solvent ionic strengths of 0, 100, or 750 mM were used. The Poisson equation or the linearized Poisson−Boltzmann equation was solved using a 2 Å Stern layer and a water probe radius of 1.4 Å to describe the molecular surface. A calculation with Debye−Huckel boundary conditions in which the molecule filled 23% of the grid was used to provide the boundary condition for a final calculation in which the molecule filled 92% of the 159 × 159 × 159 grid (final grid spacing of 0.249 Å).

Accessible Surface Area Calculations. To compute solvent accessible surface areas, solvation radii from the ACCESS parameter set were assigned to each structure according to CHARMM atom type (*43*, *44*). The solvent accessible surface area was determined in CHARMM with a probe of 1.4-Å radius. The free energy contribution was taken to be 25 cal mol^{-1} Å^{-2} for the burial of surface area.

Computational Analysis of Double-Mutant Cycles. The computational calculation of the coupling free energy measured experimentally via double-mutant cycle analysis involves the sum of five terms. First, the electrostatic desolvation penalty of each of the two groups being probed ($\Delta G_i^{0desolv}$ and $\Delta G_j^{0desolv}$) was computed through differences in the bound and unbound state models of half of each group's interaction with its own reaction field. Second, electrostatic interactions between the two groups being probed ($\Delta G^{0bridge}$) were computed as the interaction of one group with the reaction field from the other. This bridge energy was independent of the group used to generate the reaction field because of reciprocity. Third, intramolecular electrostatic interactions between each of the probed groups and the rest of the protein ($\Delta G_i^{0desolv}$ and $\Delta G_j^{0desolv}$) were computed through the interaction of the bystander groups with the reaction field of each of the probe groups. Fourth, indirect effects because of changes in the interactions of bystander groups with solvent resulting from shape changes ($\Delta G^{0indirect}$) were computed through the differential interaction of the set of bystander groups with their own reaction field. Fifth, changes in the nonelectrostatic contributions ($\Delta G^{0nonelec}$) were estimated as 25 cal mol^{-1} Å^{-2} of the solvent accessible surface area difference.

RESULTS

Design and Structural Characterization of the Mutants. This study investigated a salt bridge between the side chain

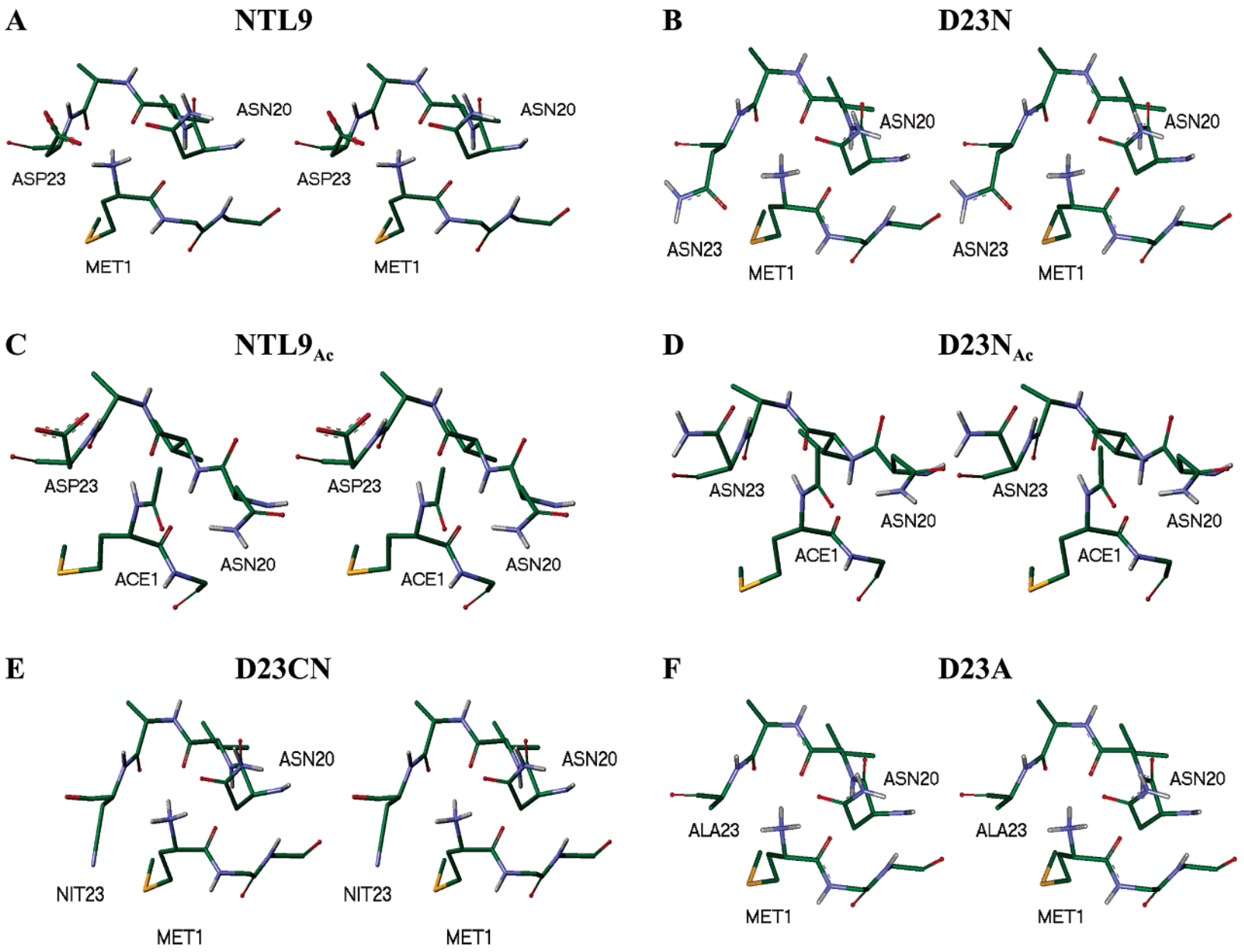

FIGURE 2: Models of mutant structures. Stereodiagrams of residues 1 and 20−23, together with the backbone of residues 2 and 3 showing the environment of the mutations from the perspective of the solvent. (A) Wild-type NTL9, (B) D23N, (C) $NTL9_{Ac}$, (D) $D23N_{Ac}$, (E) D23CN, and (F) D23A. Drawn with Weblab Viewer Lite (MSI Inc).

Table 1: Parametrization of Nitrile Alanine

	Partial charges			Force constants	
atom	CHARMM	DELPHI	radii (Å)	bond (kcal mol^{-1} Å^{-2})	bond angle (kcal mol^{-1} rad^{-2})
N	−0.35	−0.40	1.5		
H	0.30	0.40	1.0		
C_α	0.05	0.00	2.0		C_α C_β C_γ 315.0
C_β	0.16	0.16	2.0	C_β C_γ 45.0	
					C_β C_g N_δ1000.0
C_γ	0.34	0.34	1.7	C_γ N_δ 120.0	
N_δ	−0.50	−0.50	1.5		
C	0.55	0.55	1.7		
O	−0.55	−0.55	1.4		

of Asp 23 and the protonated N-terminus of the main chain. The ideal double-mutant cycle involves mutations that remove only the interaction of interest and do not alter other interactions or introduce new interactions. In practice this is often difficult to achieve, and in general it is difficult to test if these conditions, which are inherent to the analysis of all double-mutant cycles, are met. Disruption of the salt bridge was achieved by three separate changes to the aspartate side chain. Mutation to alanine removed the electrostatic interaction with the N-terminus and also eliminated the hydrogen bonding capability of the side chain. In addition, since an Ala side chain is smaller than an Asp side chain, van der Waals and solvation interactions may also have been modified, and the additional space may have permitted neighboring groups to repack. The Asn mutation was more conservative, removing the charge but preserving the ability to hydrogen bond with little change to size or shape. Using solid-phase peptide synthesis, we generated a third mutant in which Asp 23 was changed to nitrile Ala (i.e., the carboxylate group of the Asp side chain was replaced with a cyano (C≡N) group). The change removed the net charge, but nitrile Ala is still polar and is a more isosteric substitution than is Ala. It is extremely difficult to introduce a conservative mutation to the N-terminus. In an ideal scenario, the terminal amino group might be changed to a methyl group; however, this is synthetically nontrivial. Only one type of alteration was made to the N-terminus, namely, acetylation (through solid-phase synthesis), which removed the net charge but added both bulk and a potential hydrogen bond donor. All combinations of single and double mutants were prepared.

The wild-type protein is designated NTL9, and acetylated variants are denoted by an Ac subscript. The variants with Asp 23 replaced by nitrile Ala (i.e., the carboxylate replaced with a CN group) are denoted D23CN. Three double-mutant cycles were studied. The single mutants were $NTL9_{Ac}$, D23N, D23A, and D23CN, where the free N-terminus was acetylated, the aspartic acid residue was changed to an asparagine or an alanine, or the β-position of the aspartic acid was changed to a cyano group, respectively. The double mutants are designated as $D23N_{Ac}$, $D23A_{Ac}$, and $D23CN_{Ac}$; all contained an acetylated N-terminus along with the indicated substitutions at position 23. All variants were studied using 2-D ^{1}H NMR spectroscopy. The C_αH chemical shifts of the variants were all similar to the wild-type values except in the region of the mutation. The deviations in C_αH chemical shifts, excluding residues near the site of the mutation, were within 0.1 ppm of the wild-type values. In contrast, the deviation between the wild-type and the random-coil values ranged from +1.5 to −1.0 ppm. C_αH chemical shifts are very sensitive to environment, and the lack of large changes relative to the wild-type protein provided evidence that there were no major structural changes in the mutants. Wild-type chemical shifts have been reported previously; additional assignments for the alanine family of mutants are provided in the Supporting Information (*33*). Additional evidence for the structural integrity of the mutants was provided by the observation of a set of distinctive ring current shifted methyl resonances in all of the spectra. Our NMR chemical shift data do not provide detailed information about the local structure at the site of the mutation(s) but do clearly indicate that the global fold is very similar. Consequently, we used the wild-type structure to generate model structures of the various individual and double mutants. Generation of models involving nitrile alanine required the development of a set of parameters for this unnatural amino acid. The process is described in detailed in the Materials and Methods, and the parameters are listed in Table 1. Models of the mutant structures built from the combined X-ray/NMR wild-type structure are shown in Figure 2. The wild-type structure is shown in Figure 2A, the D23N mutant in Figure 2B, $NTL9_{Ac}$ in Figure 2C, and the double mutant in Figure 2D. Also shown are the models for D23CN and D23A. In the D23A model, only one interaction strongly differed from wild type, namely, the lack of an electrostatic interaction between Ala 23 and the N-terminus. The truncation of the Asp side chain also allowed for greater solvation of the N-terminus (Figure 2F). In D23N, the Asn side chain hydrogen bonded to the N-terminus (Figure 2B), but in D23CN a favorable interaction with the N-terminus was not found (Figure 2E). In all models with an acetylated N-terminus, the acetyl oriented itself to maintain a favorable polar interaction with carbonyl 21, while Asn 20 moved to allow packing of the new acetyl and to form favorable interactions with the acetyl carbonyl, Lys 2, and its own amide backbone. When rebuilt in the presence of the acetylated N-terminus, the side chain of the aspartic acid, asparagine, and nitrile alanine residue did not interact directly with the N-terminal acetyl because of steric constraints (Figure 2D).

Equilibrium Unfolding Experiments and Double-Mutant Cycle Analysis; *the Salt Bridge Has a Strong Favorable Interaction Free Energy*. The free energy of stabilization was determined by a series of urea denaturation experiments in 100 mM NaCl and 10 mM phosphate at 25 °C. Urea was used rather than guanidine hydrochloride to avoid ionic strength effects. The conditions were chosen to allow comparison with our previous investigations of this protein. The *m* values for all of the mutants were very close to the value of the wild type. *M* values report on the difference in solvent accessible surface area between the native and the unfolded states (*45*, *46*). The good agreement among the *m* values coupled with the observation that the native structures are all very similar provides some indirect evidence that the mutations do not significantly perturb the unfolded state ensemble (*47*, *48*). The stability estimated by urea denaturation agrees well with the stability extrapolated from thermal denaturation data using the Gibbs−Helmholtz relationship and with the stability estimated by amide H/D exchange measurements (*49*). Thus, urea denaturation provides a simple and robust method for estimating the stability of NTL9 and its variants.

Table 2: Summary of Equilibrium Stability Measurements for Wild-Type NTL9 and the Salt-Bridge Mutants in 10 mM Sodium Phosphate, pH 5.4 at 25 °C with (A) 100 mM NaCl or (B) 750 mM NaCl[a]

A. 100 mM NaCl

protein	T_m (°C)	ΔG_f^0 (H_2O) (kcal mol^{-1})	m (kcal mol^{-1} M^{-1})	[urea]$_{50\%}$	$\Delta\Delta G_f^0$ (H_2O) (kcal mol^{-1})
NTL9	77	-4.45 ± 0.3	0.72	6.18	
NTL9$_{Ac}$	56	-2.02 ± 0.2	0.64	3.16	2.43
NTL9 D23N	67	-3.73 ± 0.1	0.70	5.33	0.72
NTL9 D23N$_{Ac}$	57	-2.00 ± 0.3	0.68	2.94	2.45
NTL9 D23A	72	-3.99 ± 0.13	0.69	5.78	0.46
NTL9 D23A$_{Ac}$	63	-3.27 ± 0.2	0.75	4.36	1.18
NTL9 D23CN	61	-2.95 ± 0.25	0.71	4.15	1.50
NTL9 D23CN$_{Ac}$	56	-2.18 ± 0.2	0.72	3.03	2.27

B. 750 mM NaCl

protein	ΔG_f^0(H_2O) (kcal mol^{-1})	m (kcal mol^{-1} M^{-1})	[urea]$_{50\%}$	$\Delta\Delta G_f^0$(H_2O)[b] (kcal mol^{-1})
NTL9	-4.81 ± 0.16	0.62	7.76	
NTL9$_{Ac}$	-2.40 ± 0.1	0.66	3.64	2.41
NTL9 D23A	-4.30 ± 0.43	0.60	7.17	0.51
NTL9 D23A$_{Ac}$	-3.53 ± 0.2	0.69	5.12	1.28

[a] ΔG_f0 (H_2O) is the free energy of folding in the absence of denaturant. [urea]$_{50\%}$ is the concentration of urea at the midpoint of the unfolding transition. The $\pm$ values associated with each ΔG_f0 (H_2O) represent the standard error to the fit. The precision of the measured T_m's are 1.0 °C or better. [b] Relative to wild type in 750 mM NaCl (i.e., $\Delta\Delta G_f^0$ (H_2O) = ΔG_f^0 (mutant, H_2O, 750 mM NaCl) − ΔG_f^0(wild type, H_2O, 750 mM NaCl).

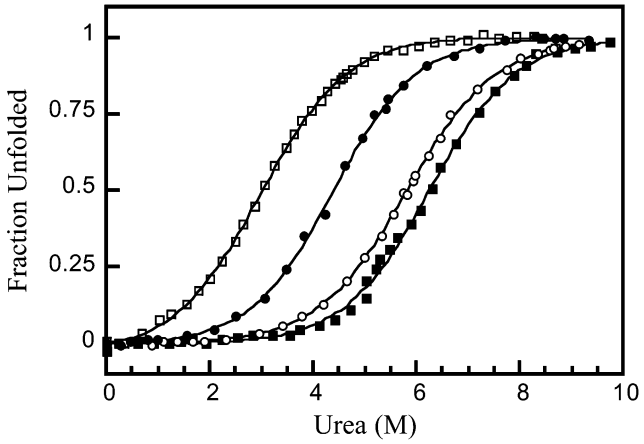

FIGURE 3: Urea unfolding curves for the Ala based family of mutants. Closed squares (■) represent the wild-type protein, NTL9$_{Ac}$ is represented by open squares (□), NTL9 D23A by open circles (○), and NTL9 D23A$_{Ac}$ by closed circles (●). The solutions contained 100 mM NaCl, 10 mM sodium phosphate in H_2O at pH 5.4. The solid lines represent nonlinear least-squares fits to the standard expression for denaturant induced unfolding.

Representative plots of the chemical denaturation experiments are shown for the alanine double-mutant cycle in Figure 3. Both the thermal and the denaturant induced unfolding transitions were reversible. All of the variants were less stable than the wild type, and the values of $\Delta G°$ are summarized in Table 2. For the Asp23 to Asn family of mutants, the decrease in T_m ranged from 10 °C for NTL9 D23N to 21 °C for NTL9 D23N$_{Ac}$. The decrease in $\Delta G°$ at 25 °C, 100 mM NaCl ranged from 2.45 kcal mol^{-1} for D23N$_{Ac}$ to 0.72 kcal mol^{-1} for the D23N mutant, the bulkiest and the most isosteric substitutions, respectively. Similar results were obtained for the other sets of mutants. In general, acetylation of the N-terminus resulted in a larger decrease in stability than did modification of the side chain of position 23. Blocking the charge on the N-terminus by acetylation significantly modulated the pK_a of Asp 23 leading to a difference of one pK_a unit between wild type (pK_a = 3.04) and the NTL9$_{Ac}$ variant (pK_a = 4.01).

The coupling free energy between the Asp 23 side chain and the free N-terminus, $\Delta\Delta G^0_{coupling}$, was calculated from the experiments using eq 1, where ΔG^0_{WT}, ΔG^0_{D23X}, ΔG^0_{Ac}, and $\Delta G^0_{D23X,Ac}$ are the free energies of folding for the wild-type protein, the two single mutants, and the double-mutant protein, respectively. The subscript D23X refers to the different replacements of the D23 side chain.

$$\Delta\Delta G^0_{coupling} = (\Delta G^0_{WT} - \Delta G^0_{D23X,Ac}) - [(\Delta G^0_{D23X} - \Delta G^0_{D23X,Ac}) + (\Delta G^0_{Ac} - \Delta G^0_{D23X,Ac})] \quad (1a)$$

The relationship can be rearranged to give the somewhat simpler form

$$\Delta\Delta G^0_{coupling} = \Delta G^0_{WT} - \Delta G^0_{D23X} - \Delta G^0_{Ac} + \Delta G^0_{D23X,Ac} \quad (1b)$$

The measured coupling free energy was found to depend on the mutants used in the analysis. Values ranged from a favorable −1.7 kcal mol^{-1} for both the alanine cycle and the nitrile alanine to a favorable −0.7 kcal mol^{-1} for the asparagine cycle. Given the estimated uncertainty in individual ΔG^0 measurements as judged by repeat measurements, typically ±0.2 kcal mol^{-1}, the −1.0 kcal mol^{-1} difference in measure coupling free energies is small but likely real. The range of measured interaction free energies are in good agreement with that expected from the pK_a shift of Asp 23 induced by acetylation of the N-terminus. Note that the observation that different choices of mutants give different coupling energies suggests that some of the basic assumptions of the double-mutant cycle analysis may not be meet. Most reported double-mutant cycles make use of only one set of mutants.

The data can rearranged to calculate the coupling free energy between the Asn 23 side chain and the N-terminus in the D23N mutant and between the cyano group and the

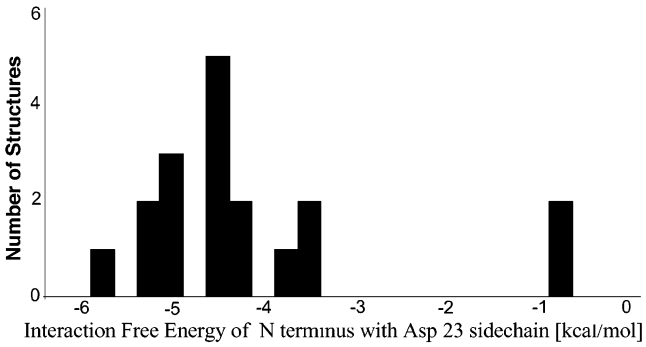

FIGURE 4: Distribution of the computed interaction free energies between the N-terminus and Asp 23 in the 18 members of the NMR structure ensemble. Two structures lack a well-formed salt bridge.

N-terminus in the D23CN variant. In this analysis, D23N assumes the role of the wild type in the calculation of the interaction free energy between the Asn side chain and the N-terminus while D23A, $D23N_{Ac}$, and $D23A_{Ac}$ are used as the two single and one double mutant. In a similar fashion, D23CN is treated as the wild type in the calculation of the interaction free energy between the cyano group and the N-terminus. The analysis is useful because it facilitates comparison with the computational studies (vide infra). The experimental coupling free energy between an Asn side chain at position 23 and the protonated N-terminus is -1.0 kcal mol^{-1}, while a value of -0.1 kcal mol^{-1} is found for the nitrile alanine N-terminus coupling free energy.

The Interaction Free Energy Calculated Using Continuum Electrostatics Calculations Is Significantly Larger than the Experimentally Determined Coupling Free Energy. Using the joint X-ray/NMR structure, the interaction free energy between the charged N-terminus and Asp 23 was computed to be a favorable -4.34 kcal mol^{-1} at 100 mM ionic strength. This is considerably larger than the experimental coupling free energy between D23 and the N-terminus measured with any of the experimental double-mutant cycles. The calculated energy term was computed using the folded state structure and is an interaction free energy rather than a coupling free energy because no double-mutant cycles were considered. Electrostatic interactions can be sensitive to small changes in the position of charged groups. Consequently, we recalculated the interaction free energy at 100 mm NaCl for the 16 structures in the NMR ensemble that form a salt bridge to ensure that our results were not biased by calculations on a single representative structure. The average interaction free energy calculated for the 16 members of the NMR ensemble that formed a salt bridge between the N-terminus and Asp 23 was -4.56 kcal mol^{-1} (favorable), with 12 of the structures falling between -4.26 and -5.36 kcal mol^{-1} (Figure 4).

Calculations were also performed to calculate the interaction free energy between an Asn at position 23 and the N-terminus and between a nitrile Ala at position 23 and the N-terminus. The interaction free energy between Asn 23 and the N-terminus was calculated to be favorable by -0.63 kcal mol^{-1} in the D23N model, which is in better agreement with the experimentally measured coupling free energy of -1.0 kcal mol^{-1}. The interaction free energy between the side chain of nitrile Ala and the N-terminus was calculated to be an unfavorable $+0.91$ kcal mol^{-1}, while the experimentally measured coupling free energy was close to zero, -0.1 kcal mol^{-1}.

The coupling free energies between D23 and the N-terminus measured experimentally were very different from the computed interaction free energies. This could be a genuine disagreement; however, it is important to re-emphasize that the values computed correspond to very different processes. Only under ideal circumstances can the coupling term be interpreted as an interaction free energy. A double-mutant cycle is designed to cancel context effects and eliminate all interactions except the interaction between the two mutated sites; however, this may not always be true in practice. For example, a mutation might alter other interactions, and the effects might be different in the double and single mutants. In this case, the effect will not be canceled by the cycle. Mutations at one site could also alter solvation effects at another site by, for example, altering the solvent accessibility of the site. This will lead to desolvation terms that do not cancel in the cycle. In addition, a mutation might introduce an additional interaction, and this new contribution to $\Delta G°$ need not be canceled out by the cycle. In general, highly conservative mutations should reduce but may not always eliminate such complications. In our case, the large size of the acetyl group and its hydrogen bonding capabilities give rise to the possibility of new interactions. Unfortunately, there are no easily accessible conservative mutations of the N-terminus. Note that even highly conservative mutations can have significant effects. For example, the analysis described in detail in the next section shows that even the very conservative Asp to Asn mutation gives rise to effects that are not canceled by the double-mutant cycle. The results are summarized in Figure 5, which compares the calculated and experimental coupling and interaction energies for the three double-mutant cycles (Figure 5A). The figure also includes the analysis of the interaction of the N-terminus with the various groups at position 23 (Asp, Asn, and nitrile Ala) (Figure 5B).

Continuum Electrostatics and Double-Mutant Cycle Calculations: Additional Interactions Introduced by Mutation Can Account for the Difference between the Calculated Interaction Free Energies and the Experimental Coupling Free Energies. To provide a better comparison between theory and experiment, we have computationally studied the mutants in the double-mutant cycle analysis to provide theoretical coupling free energies. The calculated double-mutant cycle energies included four electrostatic and one nonelectrostatic contribution, which we briefly outlined here (see also Materials and Methods). Desolvation contributions ($\Delta G_i^{0desolv}$ and $\Delta G_j^{0desolv}$) accounted for differences in the desolvation penalties of the pair of groups. Bridge interactions ($\Delta G^{0bridge}$) accounted for interactions between the pair of groups. Intramolecular electrostatic interaction contributions (ΔG_i^{0intra} and ΔG_j^{0intra}) accounted for their interactions with groups that remained invariant throughout the double-mutant cycle (bystander groups). The movement of the dielectric boundary can result in a surface area correction, a change in side chain−protein interactions, and even small protein−protein interaction changes. Indirect contributions ($\Delta G^{0indirect}$) were due to changes in the interactions of bystander groups with solvent. Finally, nonelectrostatic contributions ($\Delta G^{0nonelec}$) were computed through changes

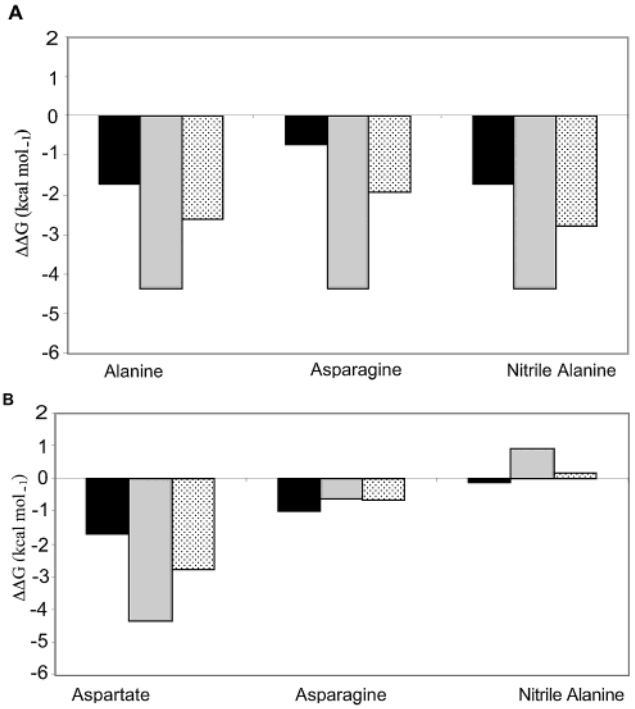

FIGURE 5: Summary of the analysis of the coupling terms. (A) Analysis of the interaction of Asp 23 with the N-terminus using the three double-mutant cycles. The identity of the cycle is indicated on the *X* axis and is identified by the substitution used at residue 23. The bar graphs represent the experimental or calculated interaction and coupling free energies. The left column (black) represents the experimental coupling free energy, the middle column (gray) represents the computed interaction free energy, and the right column (dots) represents the computed coupling free energy. (B) Comparison of the experimental and calculated interaction and coupling free energies for the interaction between the N-terminus and the various side chains at residue 23. The *X* axis is labeled with the identity of the group at position 23. From left to right: interaction of Asp-23 with the N-terminus, interaction of Asn-23 with the N-terminus, and interaction of nitrile alanine-23 with the N-terminus. In each set, the black column represents the experimental coupling free energy, the middle column (gray) represents the computed interaction free energy, and the right column (dots) represents the computed coupling free energy. Alanine double-mutant cycles were used to derive the coupling and interaction energies.

in solvent accessible surface area. The net $\Delta\Delta G^0_{\text{intereaction}}$ measured via a double-mutant cycle is the sum of these contributions

$$\Delta\Delta G^0_{\text{intereaction}} = \Delta\Delta G^{0\ \text{desolvation}}_{\text{Nter}} + \Delta\Delta G^{0\ \text{desolvation}}_{\text{D23X}} + \Delta\Delta G^{0\text{bridge}} + \Delta\Delta G^{0\ \text{intra}}_{\text{Nter}} + \Delta\Delta G^{0\ \text{intra}}_{\text{D23X}} + \Delta\Delta G^{0\ \text{indirect}} + \Delta\Delta G^{0\text{nonelec}} \quad (2)$$

The values of the various $\Delta\Delta G°$ terms are listed in Table 3 for each of the double-mutant cycles. Each term in eq 2 represents the contribution summed over the double-mutant cycle. For example, the contribution of the desolvation of the N-terminus for the alanine cycle, $\Delta G^{0\ \text{desolvation}}_{\text{Nter}}$, is given by

$$\Delta\Delta G^{0\ \text{desolvation}}_{\text{Nter}} = \Delta G^{0\ \text{desolvation}}_{\text{Nter}}(\text{NTL9}) - \Delta G^{0\ \text{desolvation}}_{\text{Nter}}(\text{D23A}) - \Delta G^{0\ \text{desolvation}}_{\text{Nter}}(\text{NTL9}_{\text{Ac}}) + \Delta G^{0\ \text{desolvation}}_{\text{Nter}}(\text{D23A}_{\text{Ac}}) \quad (3)$$

Table 3: Contribution of Free Energy Components ($\Delta\Delta G^0$) to Apparent Coupling Terms Measured via Double-Mutant Cycle Analysis[a]

double-mutant cycle	D23X═A	D23X═N	D23X═CN	N23A	CN23A
Desolvation of the N-terminus					
$\Delta\Delta G^{0\ \text{desolv}}_{\text{Nter}}$	1.3	0.9	1.2	0.4	0.0
Desolvation of the side chain of residue 23					
$\Delta\Delta G^{0\ \text{desolv}}_{\text{D23X}}$	0.4	0.3	0.4	0.1	-0.1
Bridge term between the side chain of residue 23 and the N-terminus					
$\Delta\Delta G^{0\ \text{bridge}}$	−4.0	−3.3	−4.5	−0.6	0.5
Interaction of the N-terminus with other groups in protein					
$\Delta\Delta G^{0\ \text{intra}}_{\text{Nter}}$	−0.4	0.0	−0.1	−0.4	−0.3
Interaction of the side chain of residue 23 with other groups in protein					
$\Delta\Delta G^{0\ \text{intra}}_{\text{D23X}}$	0.5	0.1	0.6	0.4	−0.1
Indirect interactions					
$\Delta\Delta G^{0\ \text{indirect}}$	−0.1	0.3	−0.2	−0.4	0.0
Nonelectrostatic interactions					
$\Delta\Delta G^{0\ \text{nonelec}}$	−0.3	−0.2	−0.4	−0.1	-0.1
total theoretical $\Delta\Delta G^0$	−2.6	−1.9	−2.8	−0.7	0.2
experimental $\Delta\Delta G^0$	−1.7	−0.7	−1.7	−1.0	−0.1

[a] The net result for a calculated double-mutant cycle is obtained by summing all of the terms in one column. The final result is included and is listed as theoretical $\Delta\Delta G°$ coupling. The experimental values are included for comparison. Units are kcal mol^{-1}. The first three columns represent the calculations for the coupling free energy between D23 and the N-terminus using three different double-mutant cycles. From right to left, the cycles are the D23 to Ala cycle (D23X═A), the D23 to Asn cycle (D23X═N), and the D23 to a nitrile Ala cycle (D23X═CN). The last two columns represent the calculation of the coupling free energy between an Asn (N23A) or a nitrile Ala (CN23A) at position 23 and the N-terminus. These calculations are considered double-mutant cycles in which the side chain at position 23 was mutated to Ala.

The individual terms in eq 3 ($\Delta G°$ values) that contribute to each of the $\Delta\Delta G°$ terms in eq 2 are given in Table 4.

It is useful to describe the results for one cycle in detail. We consider the D23A cycle as an example. The analysis shows the N-terminus paid a 7.7 kcal mol^{-1} desolvation penalty in the wild-type model and a 6.4 kcal mol^{-1} desolvation penalty when Asp 23 was truncated to Ala. The uncharged, bulkier, acetylated N-terminus paid about 2 kcal mol^{-1} in desolvation regardless of the side chain at position 23. This means that there will be a 1.3 kcal mol^{-1} contribution from the differences in the desolvation of the N-terminus, which is not canceled by the cycle. The net effect of uncanceled desolvation terms on the double-mutant cycle coupling free energy was 1.3 kcal mol^{-1} for the N-terminus and 0.4 kcal mol^{-1} for residue 23 (Table 3). The bridge interaction was −4.34 kcal mol^{-1} in the wild type and zero in D23A and D23A$_{\text{Ac}}$ but was nonzero in NTL9$_{\text{Ac}}$. The value, −0.36 kcal mol^{-1}, represents another contribution that is not canceled by the double-mutant cycle. This will result in a positive contribution to the calculated cycle since the free energy terms associated with the single mutants are subtracted during the cycle. The intramolecular interactions of Asp 23 with invariant groups also did not cancel over the cycle. There was a difference between the wild type (−1.0 kcal mol^{-1}) and the acetylated (−1.5 kcal mol^{-1}) backgrounds, leading to an addition + 0.5 kcal mol^{-1} correction. There was a −0.4 kcal mol^{-1} contribution from variations

Table 4: Analysis of the Contributions of Each Protein Variant to the Double-Mutant Cycle Free Energy Components Given in Table 3[a]

double-mutant cycle	D23X═A	D23X═N	D23X═CN	N23A	CN23A
Desolvation of N-terminus					
$\Delta G^0_{WT}{}^{desolv}$	7.7	7.7	7.7	6.8	6.5
$\Delta G^0_{D23X}{}^{desolv}$	6.4	6.8	6.5	6.4	6.4
$\Delta G^0_{Ac}{}^{desolv}$	2.0	2.0	2.0	2.0	2.0
$\Delta G^0_{Ac,D23X}{}^{desolv}$	2.0	2.0	2.0	2.0	2.0
$Net\Delta\Delta G^0_{Nter}{}^{desolv}$	1.3	0.9	1.2	0.4	0.0
Desolvation of the side chain of residue 23					
$\Delta G^0_{WT}{}^{desolv}$	1.3	1.3	1.3	0.4	0.2
$\Delta G^0_{D23X}{}^{desolv}$	0.0	0.4	0.2	0.0	0.0
$\Delta G^0_{Ac}{}^{desolv}$	0.9	0.9	0.9	0.3	0.3
$\Delta G^0_{Ac,D23X}{}^{desolv}$	0.0	0.3	0.3	0.0	0.0
$Net\Delta\Delta G^0_{D23X}{}^{desolv}$	0.4	0.3	0.4	0.1	−0.1
Bridge term between the side chain of residue 23 and the N-terminus					
$\Delta G^0_{WT}{}^{bridge}$	−4.3	−4.3	−4.3	−0.6	0.9
$\Delta G^0_{D23X}{}^{bridge}$	0.0	−0.6	0.9	0.0	0.0
$\Delta G^0_{Ac}{}^{bridge}$	−0.4	−0.4	−0.4	0.0	0.4
$\Delta G^0_{Ac,D23X}{}^{bridge}$	0.0	0.0	0.4	0.0	0.0
$Net\Delta\Delta G^{0\ bridge}$	−4.0	−3.3	−4.5	−0.6	0.5
Interaction of the N-terminus with other groups in protein					
$\Delta G^0_{WT}{}^{intra}$	−3.0	−3.0	−3.0	−3.0	−3.0
$\Delta G^0_{D23x}{}^{intra}$	−2.8	−3.0	−3.0	−2.8	−2.8
$\Delta G^0_{Ac}{}^{intra}$	−1.9	−1.9	−1.9	−1.9	−2.0
$\Delta^0 G_{Ac,D23X}{}^{intra}$	−2.1	−1.9	−2.0	−2.1	−2.1
$Net\Delta\Delta G^0_{Nter}{}^{intra}$	−0.4	0.0	−0.1	−0.4	−0.3
Interaction of the side chain of residue 23 with other groups in protein					
$\Delta G^0_{WT}{}^{intra}$	−1.0	−1.0	−1.0	−0.2	0.3
$\Delta G^0_{D23X}{}^{intra}$	0.0	−0.2	0.3	0.0	0.0
$\Delta G^0_{Ac}{}^{intra}$	−1.5	−1.5	−1.5	−0.6	0.4
$\Delta G^0_{D23X,Ac}{}^{intra}$	0.0	−0.6	0.4	0.0	0.0
$Net\Delta\Delta G^0_{D23X}{}^{intra}$	0.5	0.1	0.6	0.4	−0.1
Net indirect terms					
$\Delta\Delta G^{0indirect}$	−0.1	0.3	−0.2	−0.4	0.0
Net nonelectrostatic contributions					
$\Delta\Delta G^{0nonelec}$	−0.3	−0.2	−0.4	−0.1	0.1

[a] The double-mutant cycles are labeled as in Table 3. All units are kcal mol^{-1}. The net contribution to the double-mutant cycle for a given component is a $\Delta\Delta G°$ defined as $\Delta\Delta G°^{componet} = \Delta G^0_{WT}{}^{componet} - \Delta G^0_{D23X}{}^{component} - \Delta G^0_{Ac}{}^{componet} + \Delta G^0_{Ac,D23X}{}^{componet}$.

in the intermolecular interactions between the N-terminus and the rest of the protein. Indirect effects nearly canceled in the cycle (the net effect was only −0.1 kcal mol^{-1}), and nonelectrostatic effects accounted for another −0.3 kcal mol^{-1} deviation from ideal behavior. Note that all of these terms represent contributions to the free energy that should be canceled by the cycle but are not. The net effect for the cycle is a $(1.3 + 0.4 + 0.36 + 0.5 - 0.4 - 0.1 - 0.3) =$ +1.76 kcal mol^{-1} correction. Addition of this correction to the calculated bridge term, −4.34 kcal mol^{-1}, gives a quantity that represents the computational version of the actual experimental double-mutant cycle. Thus the result, −2.6 kcal mol^{-1}, can be compared with the actual experimental value of −1.7 kcal mol^{-1}.

In summary, the double-mutant cycle energy contributions sum to form apparent coupling terms that resemble the experimental coupling terms. The effect of considering double-mutant cycle contributions is considerable, making the wild-type salt bridge appear less favorable, while masking an unfavorable match between the N-terminus and the nitrile alanine mutant. The calculations reproduce the experimentally observed trend of similar values for the alanine and nitrile alanine cycle and a less favorable coupling term for the asparagine cycle (Figure 5).

The Interaction between Asp-23 and the N-Terminus Is Not Screened by High Salt. The experimental coupling free energy was also measured at 750 mM NaCl using the alanine cycle. Interestingly, although a clear electrostatic interaction is visible in the structure, the corresponding experimentally determined coupling free energy is essentially unscreened by increasing the ionic strength between 100 and 750 mM. The stability for all four of the variants increased slightly with an increase in ionic strength, typically by 0.26 to 0.4 kcal mol^{-1}. However, the coupling free energy measured in high salt for the alanine cycle, −1.6 kcal mol^{-1}, was virtually identical to the value measured in low salt, −1.7 kcal mol^{-1}. The salt dependence of the interaction free energy for the folded state structure was calculated using continuum electrostatics. The strength of the interaction was calculated to be −4.61 kcal mol^{-1} at 0 M ionic strength, −4.34 kcal mol^{-1} at 100 mM ionic strength, and −4.13 kcal mol^{-1} at 750 mM ionic strength.

These calculations yield the interaction free energy but not the coupling free energy (i.e., they do not include the double-mutant cycle corrections described in the previous section). Consequently, we repeated the entire double-mutant cycle calculation for the alanine cycle at 750 mM. The only component to change with increasing salt was the direct coupling term between the two charged species Asp 23 and the N-terminus; however, the effects were small. The reduction in both the interaction free energy and the computed coupling free energy was only about 0.2 kcal mol^{-1}. Although the lack of screening may seem surprising, there is precedence for weak ionic strength effects on surface salt bridges. Early studies by Pertuz and co-workers noted that a His Asp surface salt bridge in human hemoglobin was insensitive to ionic strength, as judged by the lack of salt dependence of the His pK_a (*50*). Recently, Garcia-Morenao and co-workers have reported a series of detailed continuum electrostatic calculations on the effect of ionic strength on pK_as and electrostatic interactions in several proteins (*15*, *51*, *52*). One of their studies examined a surface salt bridge in myoglobin. Like the results reported here, they found that the strength of that salt bridge, as judged by pK_a shifts, was largely insensitive to salt (*15*). In addition, and in agreement with our analysis, their study of this salt bridge found no effect of salt on the desolvation terms, and they observed that the small effects of increasing ionic strength were confined to the coupling term.

Changes in the structure and energetics of the unfolded state induced by the mutants are not accounted for in the double-mutant cycle analysis. Potential unfolded state effects have been almost universally ignored in double-mutant analysis, but it is worth noting the complications that they might cause. Problems can arise if the mutations modify unfolded state structure in a way that is not canceled out by the mutant cycle. There are two lines of indirect experimental evidence that argue that changes in unfolded state interactions do not play a significant role for the salt bridge under investigation here. First, the *m* values for the equilibrium unfolding are similar. Since the native state structure is not significantly perturbed, this implies that there are not large changes in the denatured state as have, for example, been observed with *S.* nuclease (*47*). Second, and of greater

importance, we have previously shown that residual electrostatic interactions in the denatured state of NTL9 are effectively screened by high salt (*35*). Our observation that the calculated and measured interaction free energies are insensitive to salt again suggests that unfolded state effects are not critical. In principle, electrostatic interactions in the unfolded state can be probed by comparing the pH dependence of $\Delta G°$ of folding for the wild type and for a set of point mutants in which the ionizable residues are individually mutated to neutral residues (*53*). Analysis of the pH dependence of $\Delta G°$ of folding for the D23A mutant indicates that removal of the charged side chain does not significantly perturb unfolded state interactions (*54*).

DISCUSSION

The three objectives of this study were to investigate the role of the salt bridge between Asp 23 and the free N-terminus on the stability NTL9, to examine the validity of the standard assumptions made in double-mutant cycle analysis, and to examine the ionic strength dependence of a surface salt bridge. Three sets of double-mutant cycles were employed. The coupling free energy of the salt bridge was measured using the different cycles and the value, while always favorable, spanned 1 kcal mol^{-1} (-0.7 to -1.7 kcal mol^{-1}).

The Asp 23 to N-terminus coupling free energy is large and favorable in contrast to other experimental studies, which have shown that the coupling free energy of most solvent-exposed salt bridges are weak. There are two likely factors that contribute to the high favorable interaction free energy. First, although the residues are on the surface, they are not completely solvent exposed, and the N-terminus is significantly protected from solvent. Second, the salt bridge involves interactions between the mainchain and the backbone. The N-terminus is well-constrained by the rest of the protein, and only Asp 23 must be immobilized to form the salt bridge. An Asp side chain also has fewer degrees of freedom than a Glu. Hence, the entropic cost of forming the salt bridge is reduced. Similar observations have recently been made using a hyperthermophilic rubredoxin variant (*32*). In that study, a side chain to side chain salt bridge was found to have no contribution to the overall stability of the protein while a main chain to side chain salt bridge had a favorable -1.5 kcal mol^{-1} interaction energy.

A very small decrease in the experimental coupling free energy of approximately 0.1 kcal mol^{-1} was observed upon increasing the ionic strength from 100 to 750 mM. This is in excellent agreement with our calculations, which predicted a decrease in the interaction energy of about 0.2 kcal mol^{-1} over this range of ionic strength and with the observations of Garcia-Morenao and colleagues on myoglobin (*15*). Several factors likely contribute to the lack of salt dependence observed here. The two charged groups are very close to each other reducing the effectiveness of the screening by salt. The salt bridge interaction involves residues that are not fully solvent exposed and lie on the surface of the protein. Coulombic interactions occurring through the protein medium are less sensitive to salt since counterions cannot penetrate into the protein. There have been several other reports of ion pair interactions that are insensitive to salt, and one possible explanation that has been offered for these observations is that the interactions may behave more like hydrogen bonds then like Coulombic interactions between two charges. The experimental data and calculations reported here for NTL9 and the work of Garcia-Moreno and colleagues on myoglobin demonstrate, however, that surface salt bridges can be insensitive to salt even when there is a clear Coulombic interaction. Thus, caution needs to be employed when using ionic strength dependent effects to partition interactions between classic Coulombic and hydrogen bond interactions.

The interaction free energy of the Asp-23 N-terminus salt bridge is clearly strong and favorable but does that mean the salt bridge makes a net favorable contribution to the free energy balance of folding? This is partially a question of defining the reference state for the comparison (*6*, *14*). For mutation to two hydrophobic isosteric residues and assuming that the groups are fully solvated in the unfolded state, the answer is calculated to be no. The net contribution to the folding free energy is simply the sum of each groups' desolvation penalty, each groups interaction energies with the rest of the protein, and the coupling term. The net contribution calculated using the formulation of continuum electrostatics employed here (solvent dielectric of 80, protein dielectric of 4) is 0.63 kcal mol^{-1} unfavorable. Different computational protocols could, of course, give different answers, but the key point is that the coupling free energy, measured either experimentally or computationally, does not represent the contribution of a salt bridge to $\Delta G°$ of folding (*6*, *14*).

The experimental and theoretical analysis presented here demonstrates that the implicit assumptions inherent to all double-mutant cycles are not always met. The removal or replacement of an important interacting partner, especially for surface residues, can lead to changes that do not cancel across the double-mutant cycle as illustrated in this work. Some, but not all, of the difficulties encountered in the present case are caused by the inability to generate a conservative isosteric substitution for the protonated N-terminus. Similar difficulties will arise when analyzing interactions that involve the C-terminus of a protein. It is worth noting that the interaction between two completely buried side chains could likely be more accurately reproduced with an experimental double-mutant cycle because desolvation effects would be more likely to cancel and because the protein backbone would not need to be modified.

ACKNOWLEDGMENT

We thank Dr. Satoshi Sato for many helpful discussions and for assistance with MALDI-TOF measurements.

SUPPORTING INFORMATION AVAILABLE

Tables of ^{1}H chemical shift assignments for the D23A set of variant proteins. This material is available free of charge via the Internet at http://pubs.acs.org.

REFERENCES

1. Warshel, A., and Aqvist, J. (1991) *Annu. Rev. Biophys. Biophys. Chem. 20*, 267−298.
2. Honig, B., and Nicholls, A. (1995) *Science* 268, 1144−1149.
3. Antosiewicz, J. A., McCammom, J. A., and Gilson, M. K. (1994) *J. Mol. Biol. 238*, 415−436.

4. Bashford, D., and Karplus, M. (1991) *J. Phys. Chem. 95*, 9556−9561.
5. Matthew, J. B., Gurd, F. R. N., Garcia-Moreno, B. E., Flanagan, M. A., March, K. L., and Shire, S. J. (1985) *CRC Crit. Rev. Biochem. 18*, 91−197.
6. Forsyth, W. R., Antosiewiez J. M., and Robertson, A. D. (2002) *Proteins: Struct., Funct., Genet. 48*, 388−403.
7. Oliveberg, M., and Fersht, A. R. (1996) *Biochemistry 35*, 2726−2737.
8. Tan, Y.-J., Oliveberg, M., and Fersht, A. (1996) *J. Mol. Biol. 264*, 377−389.
9. López-Arenas, L., Solís-Mendiola, S., and Hernández-Arana, A. (1999) *Biochemistry* 38, 15936−15943.
10. Horovitz, A., Serrano, L., Avron, B., Bycroft, M., and Fersht, A. R. (1990) *J. Mol. Biol. 216*, 1031−1044.
11. Lumb, K. J., and Kim, P. S. (1995) *Science 268*, 436−439.
12. Sali, D., Bycroft, M., and Fersht, A. R. (1991) *J. Mol. Biol. 220*, 779−788.
13. Scholtz, J. M., Qian, H., Robbins, V. H., and Baldwin, R. L. (1993) *Biochemistry 32*, 9668−9676.
14. Hendsch, Z. S., and Tidor, B. (1994) *Protein Sci. 3*, 211−226.
15. Kao, Y.-H., Fitch, C. A., Bhattacharya, S., Sarkisian, C. J., Lecomte, J. T. J., and Garcia-Moreno, B. E. (2000) *Biophys. J. 79*, 1637−1654.
16. Waldburger, C. D., Schildbach, J. F., and Sauer, R. T. (1995) *Nat. Struct. Biol. 2*, 122−128.
17. Takano, K., Tsuchimori K., Yamagata Y., and Yutani, K. (2000) *Biochemistry 39*, 12375−12381.
18. Wimley, W. C., Gawrisch, K., Creamer, T. P., and White, S. H. (1996) *Proc. Natl. Acad. Sci. U.S.A. 93*, 2985−2990.
19. Elcock, A. H. (1998) *J. Mol. Biol. 284*, 489−502.
20. Korndorfer, I., Steipe, B., Huber, R., Tomschy, A., and Jaenicke, R. (1995) *J. Mol. Biol. 246*, 511−521.
21. Vogt, G., Woell, S., and Argos, P. (1997) *J. Mol. Biol. 269*, 631−643.
22. Kumar, S., Ma, B. Y., Tsai, C. J., and Nussinov, R. (2000) *Proteins: Struct., Funct., Genet. 38*, 368−383.
23. Xiao, L., and Honig, B. (1999) *J. Mol. Biol. 289*, 1435−1444.
24. Grimsley, G. R., Shaw, K. L., Fee, L. R., Alston, R. W., Huyghues-Despointes, B. M. P., Thurlkill, R. L., Scholtz, J. M., and Pace, C. N. (1999) *Protein Sci. 8*, 1843−1849.
25. Loladze, V. V., Ibarra-Molero, B., Sanchez-Ruiz, J. M., and Makhatadze, G. I. (1999) *Biochemistry 38*, 16419−16423.
26. Spector, S., Wang, W., Carp, S. A., Robblee, J., Hendsch, Z. S., Fairman, R., Tidor, B., and Raleigh, D. P. (2000) *Biochemistry 39*, 872−879.
27. Sanchez-Ruiz, J. M., and Makhatadze, G. I. (2001) *Trends Biotechnol. 19*, 132−135.
28. Perl, D., Mueller, U., Heinemann. U., and Schmid, F. X. (2000) *Nat. Struct. Biol. 7*, 380−383.
29. Serrano, L., Horovitz, A., Avron, B., Bycroft, M., and Fersht, A. R. (1990) *Biochemistry 29*, 9343−9352.
30. Anderson, D. E., Becktel, W. J., and Dahlquist, F. W. (1990) *Biochemistry 29*, 2403−2408.
31. Dao-Pin, S., Sauer, U., Nicholson, H., and Matthews, B. W. (1991) *Biochemistry 30*, 7142−7153.
32. Strop, P., and Mayo, S. L. (2000) *Biochemistry 39*, 1251−1255.
33. Kuhlman, B., Boice, J. A., Fairman, R., and Raleigh, D. P. (1998) *Biochemistry 37*, 1025−1032.
34. Luisi, D. L., and Raleigh, D. P. (2000) *J. Mol. Biol. 299*, 1091−1100.
35. Kuhlman, B., Luisi, D. L., Young, P., and Raleigh, D. P. (1999) *Biochemistry 38*, 4896−4903.
36. Pace, C. N., Shirely, B. A., and Thomson, J. A. (1989) In *Protein Structure: A Practical Approach*, Oxford University Press, Oxford England.
37. Brooks, B. R., Bruccoleri, R. E., Olafson, B. D., States, D. J., Swaminathan, S., and Karplus, M. (1983) *J. Comput. Chem. 4*, 187−217.
38. Bayly, C. I., Cieplak, P., Cornell, W. D., and Kollman, P. A. (1993) *J. Phys. Chem. 97*, 10269−10280.
39. Gilson, M. K., and Honig, B. H. (1988) *Proteins: Struct., Funct., Genet. 4*, 7−18.
40. Gilson, M. K., Sharp, K. A., and Honig, B. H. (1988) *J. Comput. Chem. 9*, 327−335.
41. Hendsh, Z. S., Sindelar, C. V., and Tidor, B. (1998) *J. Phys. Chem. B102*, 4404−4410.
42. Sitkoff, D., Sharp, K. A., and Honig, B. (1994) *J. Phys. Chem. 98*, 1978−1988.
43. Lee, B., and Richards, F. M. (1971) *J. Mol. Biol. 55*, 379−400.
44. Eisenberg, D., and McLachlan, A. D. (1986) *Nature 319*, 199−203.
45. Tanford, C. (1970) *Adv. Protein Chem. 24*, 1−95.
46. Myers, J. K., Pace, C. N., and Scholtz, J. M. (1995) *Protein Sci. 4*, 2138−2148.
47. Shortle, D. (1995) *Adv. Protein Chem. 46*, 217−247.
48. Pace, C. N., and Shaw, K. L. (2000) *Proteins: Struct., Funct., Genet. Suppl. 4*, 1−7.
49. Vugmeyster, L., Kuhlman, B., and Raleigh, D. P. (1998) *Protein Sci. 7*, 1994−1997.
50. Perutz, M. F., Gronenborn, A. M., Clore, G. M., Fogg, J. H., and Shih, D. T.-B. (1985) *J. Mol. Biol. 183*, 491−498.
51. Lee, K. K., Fitch, C. A., and Garcia-Moreno, B. E. (2002) *Protein Sci. 11*, 1004−1016.
52. Lee, K. K., Fitch, C. A., Lecomte, T. J., and Garcia-Moreno, B. E. (2002) *Biochemistry 41*, 5656−5667.
53. Oliveberg, M., Arcus, V. L., and Fersht, A. R. (1995) *Biochemistry 34*, 9424−9433.
54. Luisi, D. L. (2000) Ph.D. Thesis, Department of Chemistry, State University of New York at Stony Brook, Stony Brook, NY.

BI027202N